Article

Synergistic Effects of Plasmonic Gold and Perovskite-Type SrTiO₃ for Enhanced Photocatalytic Performance of TiO₂ Nanotube Arrays

Published as part of The Journal of Physical Chemistry virtual special issue "125 Years of The Journal of Physical Chemistry".

Tsai-Te Wang,[||] Chao-Lung Chiang,[||] Sudhakar Narra, Jhih-Long Lin, Shao-Wen Chien, Jhin-Cheng Yu, Eric Wei-Guang Diau, Yan-Gu Lin,* and M. C. Lin*

Read Online

ACCESS | Metrics & More | Article Recommendations | Supporting Information

ABSTRACT: Hydrogenated SrTiO₃/TiO₂ (H:(STO/TiO₂)) with unique heterostructured arrays was prepared, followed by the immobilization of plasmonic Au nanoparticles to form robust composite photoelectrodes. The synergistic effects of heterocoupling of perovskite-type STO on TiO₂ nanotube arrays and plasmonic Au-decoration substantially improved the photocatalytic performance with visible light. In contrast to pure TiO₂, H:(STO/TiO₂) facilitated an efficient transfer of electrons between STO and TiO₂, and decreased the recombination ratios of photoexcited electron−hole pairs. Plasmonic Au also effectively boosted the photoresponse under irradiation with visible light. Photocurrent density of 2.3 mA cm⁻² under visible light irradiation (λ > 400 nm) with IPCE peaking at 17% and a concomitant apparent quantum efficiency of 3.5% in the 580−680 nm region was achieved. Faradaic efficiency was estimated to be about 80% at the oxygen evolution rate of 18.5 μmol cm⁻² h⁻¹ under simulated sunlight irradiation (AM1.5G, 100 mW cm⁻²). With the aid of X-ray absorption spectra in situ and ultrafast transient absorption spectra, the detailed understanding of the underlying mechanism during photoinduced processes in Au/H:(STO/TiO₂) is well elucidated.
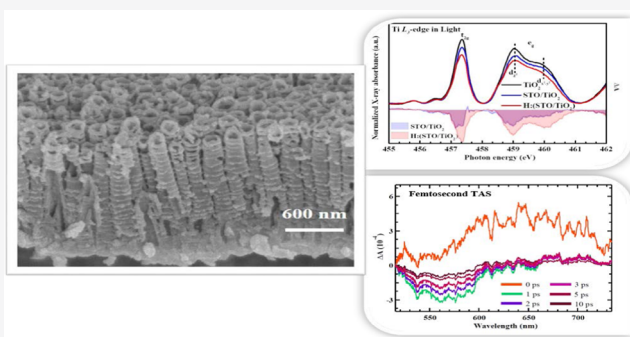
1. INTRODUCTION

In recent years, renewable energy, especially solar energy, has been regarded as a potential energy source to reduce the combustion of fossil fuels and the depletion of resources; the area of research has gained much attention.[1] The utilization efficiency of solar energy is an important issue and is of great concern. In 1972, Honda and Fujishima[2] found that hydrogen could be generated from water splitting using a TiO₂ electrode and hydrogen could be potentially employed as a clean energy source in various applications. In numerous subsequent research works, TiO₂ has been demonstrated to be photo-active, stable, nontoxic, and corrosion-resistant for energy-harvesting from solar light.[3−6] Moreover, TiO₂ with nanorod, nanowire, and nanotube shapes has been developed as an effective photoanode because of its large surface area and high efficiency of light harvesting.[6] Among these various shapes, TiO₂ with a highly ordered 1D structure can boost the electron transfer along a specific direction, thus diminishing the electron−hole recombination and enhancing the photo-conversion efficiency.[6−8] The major shortcoming of TiO₂ for solar energy harvesting, however, lies in its large band gap (∼3.2 eV) which limits its absorption of the solar light to the

UV region (λ < 380 nm), amounting to only ∼5% of the available energy in the solar spectrum.[9] To circumvent the shortcoming through the enhancement of absorption in the vis-IR range, surface modification[4,5,10] and decoration with effective light absorbers[11−14] have been made. For example, SrTiO₃ (STO), an efficient UV−vis light absorber, is well-known as an effective photoanode material because of its photoactive, chemically robust, and nontoxic properties.[15−18] On the basis of this concept, Zhang et al. tailor-designed TiO₂−STO[19] and CdS/TiO₂−STO[20] heterostructure nanotube arrays for solar energy conversion efficiency improvement. El-Sayed and co-workers[21] electrochemically fabricated Sr-doped TiO₂ nanotube array electrodes, achieving a three-fold enhancement in photoconversion efficiency over that of TiO₂ nanotube array, reaching 0.69%.
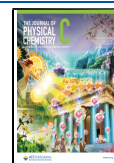
In our previous works, we have shown that hydrogenation modification of TiO_2 NPs with methanol vapor disordered the TiO_2 structure, thus enhancing the photoactivity.[10−13] It has been well demonstrated that incorporation of noble-metal particles into a material to modulate the localized surface-plasmonic resonance (LSPR) so as to extend the absorption range is also a valuable method to improve the photo-activity.[22−25] For instance, Au/TiO_2 has been shown to have a property of efficient electron−hole separation for hydrogen generation from photocatalytic water splitting.[11,15,25−28]

In the present work, we prepared a hydrogenated STO/TiO_2 (H:(STO/TiO_2)) nanotube arrays with the decoration of plasmonic Au to investigate the synergistic effects of hydrogenation modification and LSPR on the intrinsic properties and photocatalytic performance. Although the heterocoupling, hydrogenation, and the LSPR effect have been reported to enhance the photocatalytic activity, detailed understanding of the underlying mechanism during photo-induced processes in Au/H:(STO/TiO_2) remains largely inadequate. To reveal the fundamental studies of the interfacial charge transfer, tracking techniques on an atomic scale and time-resolved dynamics that allow simultaneous realization of the photochemical behaviors are highly desirable. Herein, with the aid of surface-sensitive soft X-ray techniques and bulk-information-included hard X-ray techniques at synchrotron radiation facilities, the atomic structure and electronic structure of the developed Au/H:(STO/TiO_2) are investigated in detail. Combined with ultrafast transient absorption spectroscopy, the electron dynamics behavior of the Au/H:(STO/TiO_2) has been illustrated.

2. EXPERIMENTS

2.1. Preparation of STO/TiO_2, H:(STO/TiO_2), and Au/H:(STO/TiO_2).
STO/TiO_2 was prepared via a multistep route. TiO_2 nanotubes were first grown and removed by ultrasonic on an anodized TiO_2 foil with a cavelike surface within 30 min, followed by washing with deionized water to remove unattached TiO_2. The Ti foil was subsequently immersed in an aqueous solution of $Sr(OH)_2$ (0.02−0.08 M) and aqueous NH_3F (0.2 M). The pH of the solution was adjusted to pH = 3 by dropping an appropriate volume of H_3PO_4 solute. Afterward, the STO/TiO_2 nanotubes on Ti foil were anodized at 20 V for 3 h to form an array of average tube length 1.8 μm as shown in Figure S2b. The TiO_2 nanotubes turned from silver to brown, revealing that Sr components combined successfully with TiO_2 nanotubes. Deionized water served to flush the residual solutes. The STO/TiO_2 nanotubes on Ti foil were dried in an oven at 50 °C overnight, and then crystallized by annealing in a furnace at 450 °C for 3 h, to obtain the robust STO/TiO_2 NT arrays. The STO/TiO_2 substrate was further hydrogenated under an environment of 120 Torr methanol vapor at 300 °C for 3 h until a light brown film appeared, indicating that completely hydrogenated STO/TiO_2 (H:(STO/TiO_2)) was obtained.

Before fabricating the Au/H:(STO/TiO_2), we prepared an Au hydrosol as follows. $HAuCl_4$ (5 mM) was mixed with sodium citrate ($Na_3C_6H_5O_7$, 10 mM) in a beaker; a sufficient volume of $NaBH_4$ solution at high concentration was added dropwise with vigorous stirring until the solution turned red, indicating that Au NPs (diameter 5 nm) were completely formed. The H:(STO/TiO_2) nanotube array was then immersed in this Au NP hydrosol for 12 h. Au/H:(STO/

TiO_2) was eventually obtained after annealing for 2 h at 300 °C in vacuo.

Sample Characterization. UV−vis spectra were recorded with a spectrophotometer (Hitachi U-3010) in wavelength (λ) range 250−800 nm. A fluorescence spectrometer (Edinburgh Instruments, FS5) was used to record the photoluminescence (PL) spectra. An Ar-ion laser with λ_{ex} = 514.5 nm was adopted to record Raman spectra. X-ray diffraction (XRD) patterns of prepared materials were obtained at the NSRRC beamline BL17B. High-resolution X-ray photoelectron spectra (XPS) were recorded at NSRRC BL24A1. Transmission emission microscope (TEM, JEOL JEM-ARM 200F) images were taken at the Instrumentation Center in National Yang Ming Chiao Tung University (NYCU), Hsinchu, Taiwan. Soft XAS at the Ti L-edge and the O K-edge were recorded in NSRRC at beamline TLS 20A1 equipped with a surface sensitivity of total electron yield (TEY, energy resolution $\Delta E/E \sim 1/5000$). Soft XAS of photocatalysts were recorded *in situ* under illumination with a Xe lamp incoporating a filter (AM 1.5G). The spectra of the Au L_3-edge absorption were recorded *in situ* under illumination at beamline TLS 17C. Femtosecond transient absorption spectra (TAS) were measured with a pump−probe spectrometer (ExciPro, CDP) in combination with an ultrarapid amplified laser system. The laser pulses were generated with a Ti-sapphire amplifier system (Coherent, Legend USP, 1 kHz, 795 nm, 3 mJ, 45 fs) coupled with TOPAS-C to tune the wavelength of excitation. The details of the TAS system have been published elsewhere.[64]

2.4. Photocatalytic Performance.
The photocatalytic test was measured in a self-assembled three-electrode system in a KOH (1 M)-filled enclosed glass cell. In this self-assembled three-electrode system, Au/H:(STO/TiO_2)/Ti foil, Pt plate, and Ag/AgCl served respectively as working, counter, and reference electrodes. A solar simulator (Yamashita Denso; YSS-50A) emitting AM1.5 incident light was used as a lamp, passing through a quartz window. The volume of H_2 gas generated on photolysis was collected and measured with a drainage gas system. The Faradaic efficiency of the material was evaluated on comparing the molarity of generated H_2 gas and the input charge.

■ RESULTS AND DISCUSSION

3.1. Absorption Properties.
3.1.1. UV−vis Absorbance Spectra.
The effects of STO composite formation, Au-NP loading, and hydrogenation on the band gap of the material were analyzed with absorption spectra (Figure 1a). A broad band at 350−400 nm was observed in all spectra, indicating the existence of a TiO_2 phase. With further modifications of TiO_2, the range of absorption was extended to 550−600 nm. This extension of the hydrogenation-derived band range to visible light is attributed to the corresponding created intra new bands, as systematically discussed previously.[12] The broadened absorption caused by the Au-NP loading was shifted further toward a longer wavelength, revealing an occurrence of LSPR,[11,30,31] which would explain the absorption red shift and band gap (BG) narrowing (Figure 1b). The BG variations with modifications are displayed in Figure 1b. The sequence of values of BG of these materials, derived from Tau plots, is TiO_2 (3.28 eV), STO/TiO_2 (2.88 eV), H:(STO/TiO_2) (2.58 eV), and Au/H:(STO/TiO_2) (2.24 eV). This systematically decreasing behavior was observed among the materials obtained in the formation of the STO composite, hydro-genation, and Au-NP loading process. The BG narrowing
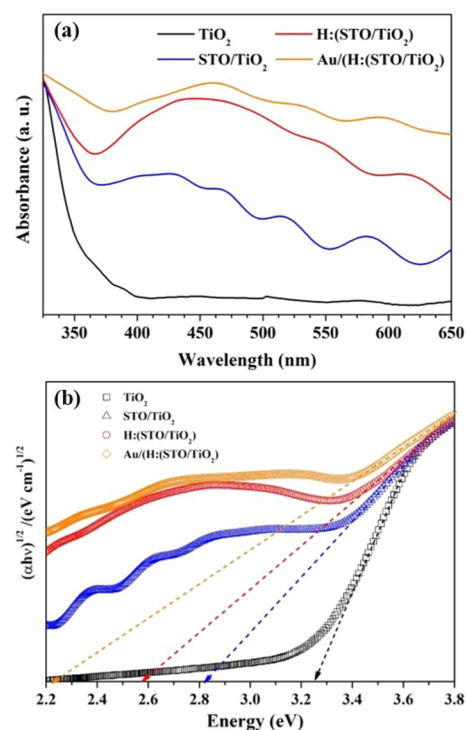
Figure 1. (a) UV−vis absorption spectra and (b) Tauc plot-derived band gap of TiO_2, STO/TiO_2, $H:(STO/TiO_2)$, and $Au/(H:(STO/TiO_2)$).

between TiO_2 and STO/TiO_2 was contributed from an intrinsic combination of STO and TiO_2 O 2p orbital.[29] The further decreased BG between STO/TiO_2 and $H:(STO/TiO_2)$ after hydrogenation is consistent with a strong absorption observed in the range of visible light (Figure 1a).

3.1.2. Raman Spectra. Figure 2 displays the intermolecular vibrational modes of the as-prepared samples, including E_g, B_{1g},
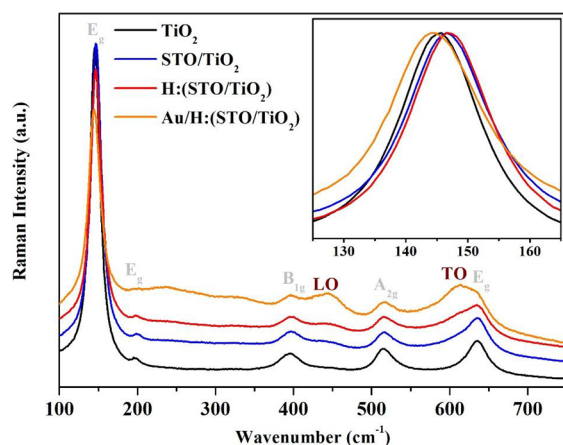

Figure 2. Raman spectra of TiO_2, STO/TiO_2, $H:(STO/TiO_2)$, and $Au/H:(STO/TiO_2)$.

and A_{2g}. Among these modes, E_g at ~145.0 cm^{-1} (inset spectrum) is a symmetric peak that is contributed from the O−Ti−O vibration.[32,33,55−57] With the STO formation and hydrogenation, the position of the E_g mode was respectively blue-shifted to 146.7 and 147.1 cm^{-1} for the STO/TiO_2 and $H:(STO/TiO_2)$ substrates, possibly related to an increased surface tension.[34] In this work, the Au vibration mode was not

detected because of the small extent of its loading. Among these spectra, a significant peak broadening and red shift toward 142.5 cm^{-1} existed for the $Au/H:(STO/TiO_2)$ substrate. The shift toward lower wavenumber is considered to result from an increased crystalline size[35] among Au deposition.[36] Aside from the E_g mode at 145.0 cm^{-1}, evident shifts appeared at the longitudinal (LO, ~445 cm^{-1}) and transverse (TO, ~615 cm^{-1}) optical modes, which are a feature of STO,[37,38] especially for $Au/H:(STO/TiO_2)$. The existence of the LO and TO modes is evidence of formation of a STO layer in the material, which was demonstrated in previous XRD patterns. Moreover, the intensity of the LO and TO modes was enhanced after Au-NP loading, which is attributed to the effect of the Au-STO junction.[30]

3.2. XRD Patterns and SEM/HRTEM Images. As exhibited in Figure S1, a typical anatase phase of TiO_2 was synthesized with the positions of the diffraction signals of TiO_2 well fitted with the standard pattern (JCPDS: 021-1272). With various modifications, the anatase phase of TiO_2 was stable. Two features of anatase phase TiO_2 at $2\theta = 38.6°$ and $40.4°$ with Miller indices (004) and (112) were identified.[39] Two other diffraction signals at $2\theta = 38.6°$ and $40.4°$ with Miller indices (004) and (111) appeared for the STO/TiO_2 substrate, indicating the existence of the STO (JCPDS: 86-0179) layer in the material, as shown in Figure 3. Compared
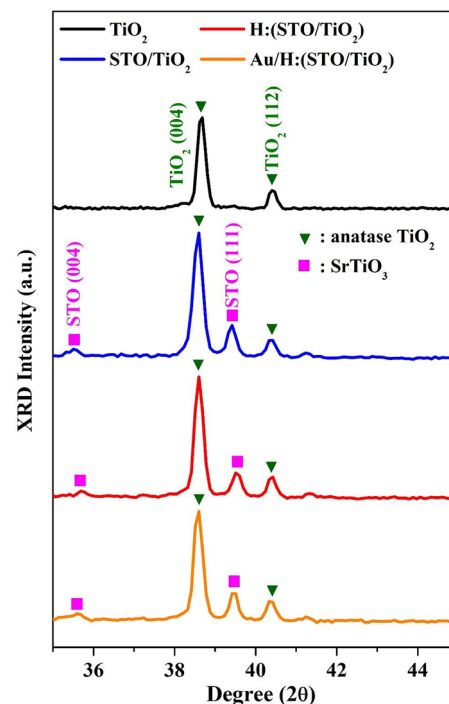

Figure 3. X-ray diffraction patterns of pristine TiO_2, STO/TiO_2, $H:(STO/TiO_2)$, and $Au/H:(STO/TiO_2)$. The diffraction signals of anatase TiO_2 (▼JCPDS, 021-1272) and STO (■JCPDS, 86-0179) were confirmed with the JPCDS database.

with TiO_2 and STO/TiO_2 materials, there is no evident shift of diffraction signal, indicating that the TiO_2 lattice is intact even after the formation of STO[21] and the Au-NP loading.[40] The configurations of $H:(STO/TiO_2)$ and $Au/H:(STO/TiO_2)$ were observed with SEM and TEM/HRTEM images. Figure S2a,b displays that the TiO_2 array was composed of uniform nanotubes of length 1.8 μm and diameter 120 nm. A random
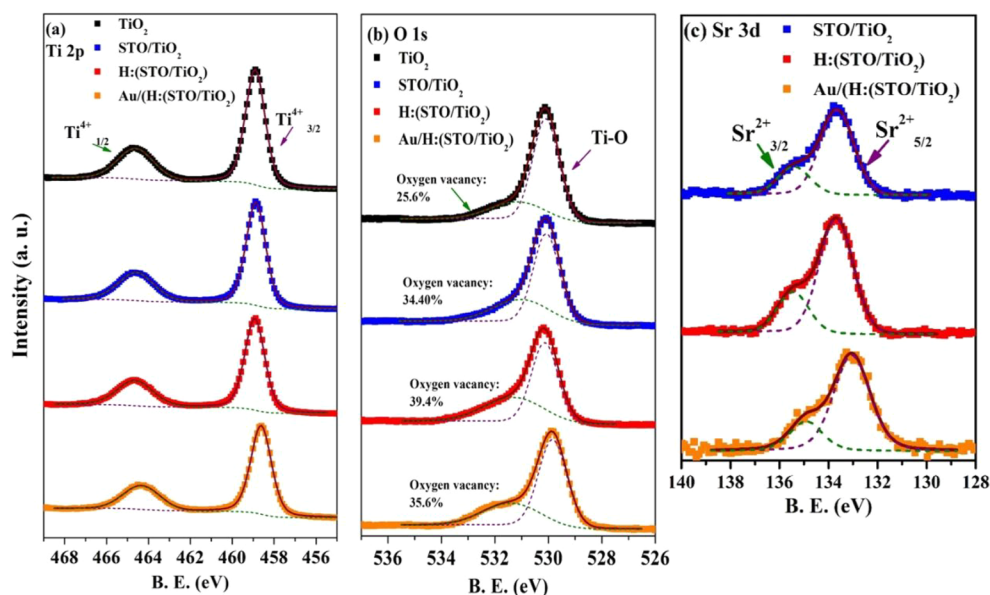
Figure 4. (a) Ti 2p, (b) O 1s, and (c) Sr 3d XPS spectra of TiO_2, STO/TiO_2, H:(STO/TiO_2), and Au/H:(STO/TiO_2).

distribution of Au NP of diameter 5 nm on the TiO_2 substrate was exhibited (Figure S2c). The *d*-spacing and Miller indices of various species on Au/H:(STO/TiO_2) were also identified (Figure S2d). The NP and substrate are respectively Au NP (*d* 0.23 nm, Miller index (111)),[14,30,40,41] STO (*d* 0.19 nm, Miller index (200)),[30,40,42] and TiO_2 (*d* 0.35 nm, Miller index (101)).[14,30]

3.3. XPS Analysis. The surface composition of Ti, O, and Sr-based species in materials was analyzed with X-ray photoelectron spectra (XPS), as shown in Figure 4a−c. Generally, the XPS of materials agreed with the fitted results, indicating the existence of Ti^{4+}-O binding in TiO_2[10,43] (Figure 4a). The lack of a Ti^{3+} feature reveals the preservation of the TiO_2 structure after the STO growth and Au-NP loading. The shifts of Ti^{4+} $2p_{3/2}$ (~458.9 eV) and Ti−O (~530.1 eV) as featured positions in various materials were not obvious (Table S1). Figure 4b shows two signals that are ascribed to the TiO_2 lattice binding (~530.1 eV) and existence of oxygen vacancies (~531.0 eV), respectively.[4,11,44] In particular, the ratio of oxygen vacancies gradually increased from 25.6% after STO formation (34.4%), hydrogenation (39.4%), and Au-NP loading (35.6%). According to the literature, the oxygen vacancies can cause band narrowing and an improved photoactivity.[11,45] Figure 4c shows two features that were assigned to Sr^{2+} $3d_{3/2}$ and Sr^{2+} $3d_{5/2}$, respectively.[21,46,47] Among the STO/TiO_2 materials, the Sr^{2+} $3d_{5/2}$ position of Au/H:(STO/TiO_2) was red-shifted to 133.15 eV, which was induced by the increased electron density.[15] The two features of Au (0) $4f_{5/2}$ (86.80 eV) and $4f_{7/2}$ (83.16 eV) indicated the existence of Au (0) NP in Au/H:(STO/TiO_2).[40,48] The atomic ratio derived from XPS is also presented in Table S1.

3.4. Gas Evolution and Photocatalytic Experiments. We used a self-assembled three-electrode system to measure the photocurrent generated from the materials. As displayed in Figure 5a, the photocurrent gradually increased with various modifications of pristine TiO_2. The photoactivity of STO/ TiO_2 (~0.60 mA/cm²) is greater than that of TiO_2 as reported.[21] After the hydrogenation, the photocurrent almost doubled (~1.20 mA/cm²), compared to that of the pristine TiO_2 (~0.30 mA/cm²). This enhanced hydrogenation-derived
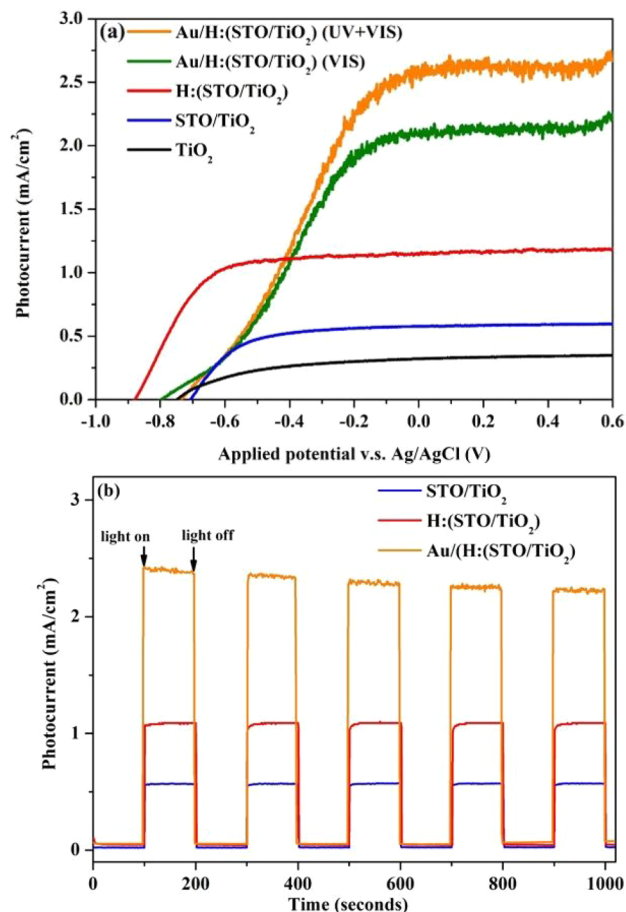

Figure 5. (a) LSV curves and (b) stability measurement of TiO_2, STO/TiO_2, H:(STO/TiO_2), and Au/H:(STO/TiO_2) in KOH (1 M) electrolyte at a constant potential of −0.2 $V_{Ag/AgCl}$ under simulated sunlight irradiation and visible-light irradiation (λ > 400 nm).

photocurrent is attributed to the suppression of charge-hole recombination[3] and the increased intraband.[12,13] The hot electrons from LSPR induced by Au NPs were measured,
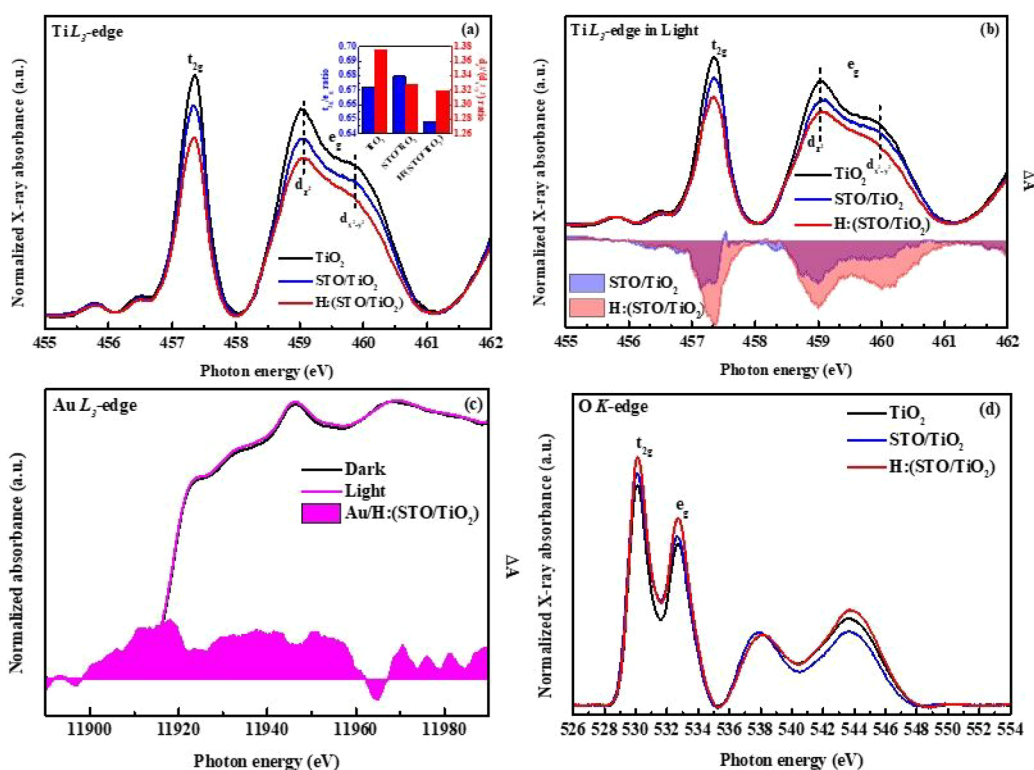
Figure 6. (a) Ti L_3-edge XAS and feature ratios (blue, t_{2g}/e_g; red, $d_{z^2}/d_{x^2-y^2}$) of pristine TiO_2, STO/TiO_2, and $H:(STO/TiO_2)$. (b) Ti L_3-edge XAS of pristine TiO_2, STO/TiO_2, and $H:(STO/TiO_2)$ under illumination. (c) Au L_3-edge XAS in situ of $Au/H:(STO/TiO_2)$ under illumination. The color-filled areas represent the intensity differences between illumination (AM1.5) and darkness states ($\Delta A = A_{illumination} - A_{darkness}$). (d) O K-edge of pristine TiO_2, STO/TiO_2, and $H:(STO/TiO_2)$.

resulting in a further enhanced photocurrent reaching 2.70 mA/cm^2. With a cutoff filter, the LSV in the visible-light range ($\lambda > 400$ nm) was also provided (Figure 5a), which demonstrates the high photoactivity of the $Au/H:(STO/TiO_2)$. Apart from the photocurrent, the durability is important for a material. As shown in Figure 5b, the photocurrent generated from materials respectively increased and decreased with and without illumination, forming several repeated pulse curves with slight photocurrent loss (<5%) and little time retard, especially $Au/H:(STO/TiO_2)$. The small photocurrent loss and little time retard of $Au/H:(STO/TiO_2)$ reveal that the charge recombination inside is suppressed and the entire photoactivity is enhanced.[30,34] In addition, the plasmonic effect of Au is verified with the incident photon conversion efficiency (IPCE) measurement, as displayed in Figure S4. The Au-photosensitized $H:(STO/TiO_2)$ displays an enhanced photoactivity in the region from 475 to 700 nm of visible light compared to $H:(STO/TiO_2)$, implying the LSPR effect is induced by Au NPs.[28,49,50] Experimentally obtained and theoretically calculated gas volumes of H_2 and O_2 produced[51,60] during solar water splitting reaction of the $Au/H:(STO/TiO_2)$ were carried out, as shown in Figure S6. The calculated Faradaic efficiency is about 80% at the oxygen evolution[60] rate of 18.5 $\mu mol\ cm^{-2}\ h^{-1}$. Meanwhile, the maximum AQE is confirmed to be 3.5% under visible light irradiation, as displayed in Figure S7.

3.5. XAS Analyses and Photocatalytic Mechanism. Aside from the photocatalytic performances and characterization results, the effects of the material modification on the intrinsic properties of TiO_2, including Ti valence, structural distortion, and oxygen vacancies, were investigated with soft

XAS. A novel technique with synchronous one-sun illumination and soft XAS was first employed for the direct observation of charge generation and transfer direction in the STO/TiO_2 photoelectrodes. As shown in Figure 6a, before irradiation with sunlight several features at 457.4, 459.1, and 459.9 eV were assigned to t_{2g} and e_g (d_{xy} and d_{yz}), which are attributed to the electron excitation from $2p_{3/2}$ (core level) to 3d (empty state) above the Fermi level. Two sub-bands (d_{z^2} and $d_{x^2-y^2}$) are split by the crystal field from e_g under the original octahedral crystal field (O_h). With the aid of the difference of band level, the outer electron configuration of titanium at the ground (Ti^{4+}, $2p^63d^0$)/excited state (Ti^{3+}, $2p^53d^1$) was identified. Moreover, the absorbance ratios t_{2g}/e_g among various materials further provide qualitative descriptions for the Ti valence and unoccupied state ratio.[51−53] As displayed in the inset of Figure 6a, the t_{2g}/e_g value increased with incorporation of strontium species and then decreased with further hydrogenation. The ratio of Ti^{3+} $3d^1$ states in STO/TiO_2 was hence greater than in other materials because of its abundant generated holes and 3d unoccupied state at the t_{2g} band. In addition, the greatest $d_{z^2}/d_{x^2-y^2}$ value of STO/TiO_2 indicates the existence of hole-induced structural asymmetry and distortion, following feature broadening called the Jahn−Teller effect.[53,54] With further hydrogenation from STO/TiO_2 to $H:(STO/TiO_2)$, the $d_{z^2}/d_{x^2-y^2}$ value further decreased because of the decreased electron energy at d_{z^2}, implying an elongation of TiO_6 along axis z and the modulation of an unoccupied state at the e_g band. In comparison with STO/TiO_2, both t_{2g}/e_g and $d_{z^2}/d_{x^2-y^2}$ values decreased after the hydrogenation, indicating that symmetry O_h was applied by an induced compressive distortion.[53] Figure 6b displays the absorbance differences among TiO_2, $STO/$
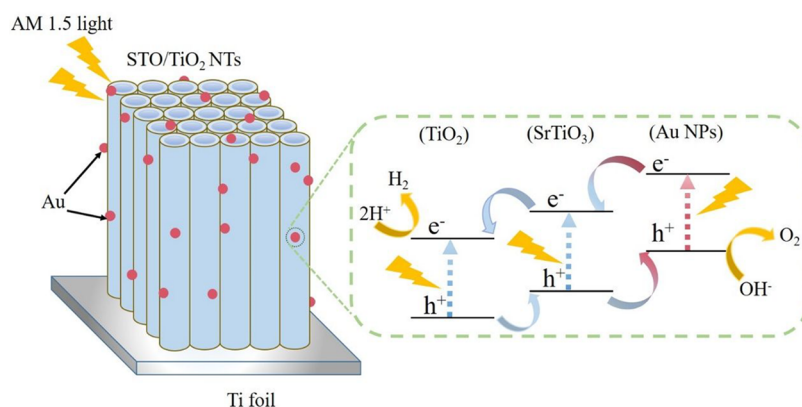
Figure 7. Schematic illustration of charge migration and separation of Au-sensitized H:(STO/TiO$_2$) heterostructured nanotube arrays.
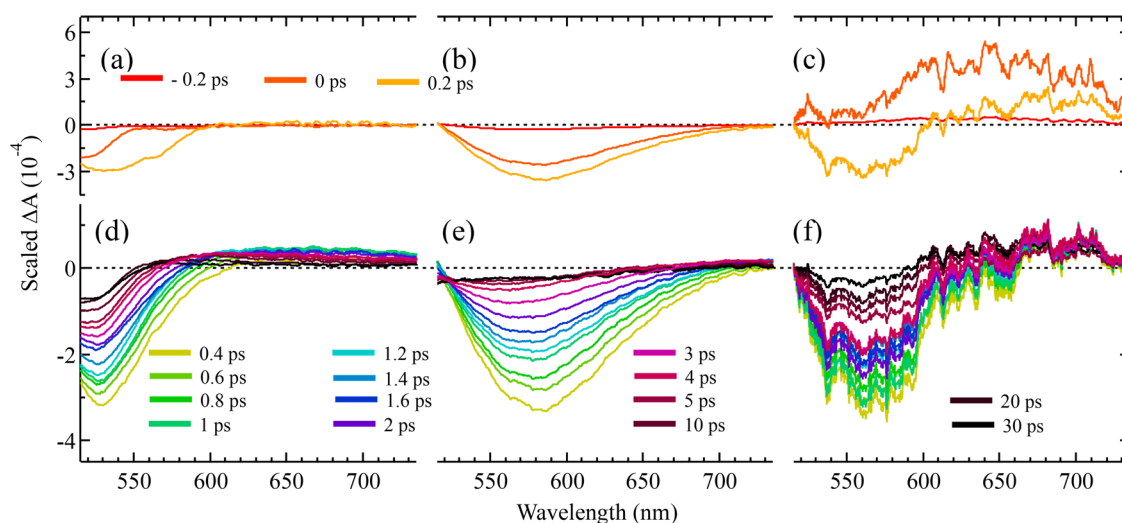

Figure 8. Femtosecond TAS of Au NP solutions (a,d), film (b,e), and Au/H:(STO/TiO$_2$) (c,f) measured using an excitation wavelength of 480 nm and pulse energy of 1.5 mJ cm^{-2}. Panels a−c show the evolution of transient absorption (TA) bands, while panels d−f show their subsequent recombination process.

TiO$_2$, and H:(STO/TiO$_2$) under sunlight illumination that are depicted in the forms of the color-filled areas (ΔA). Among these materials, the ΔA value of H:(STO/TiO$_2$) was more negative than of others, indicating that the hydrogenation modification improved the photocarrier transition and separation at the interfaces within the heterostructure.[10,52] Such a photoinduced difference is attributed to the transfer of photogenerated electrons to TiO$_2$ nanotubes, while the hydrogenated STO stored many photogenerated holes, which clearly reveal a more efficient charge separation and transfer between STO and TiO$_2$ under the sunlight irradiation. In addition, as shown in Figure 6c, further depositing Au on the surface of the H:(STO/TiO$_2$) generated the increase of unoccupied DOS of 5d-character with positive ΔA values of the Au L_3-edge XANES under solar illumination.[55] Therefore, it is significant to note that solar illumination induces the existence of hot-electron transfer from plasmonic Au to H:(STO/TiO$_2$). It is believed that *in situ* XANES provides an appropriate account of this plasmonic hot-electron transfer between the Au and H:(STO/TiO$_2$). The existence of modification-generated oxygen vacancies in the materials was confirmed from the O K-edge XAS, as exhibited in Figure 6d. Two features (t$_{2g}$ and e$_g$) are caused from the electron transitions from the ground to an unoccupied state (O 1s →

2p) and hybridization with a titanium orbital (O 2p-Ti 3d). The two featured absorbances of STO/TiO$_2$ and H:(STO/TiO$_2$) were higher than for TiO$_2$, indicating an increase of oxygen vacancies due to the presence of Ti^{3+} 3d^1 states in the unique heterostructures, which effectively promote the electrical conductivity and charge transport.[52,58,59] The increased oxygen vacancies are considered to facilitate charge separation and are thus responsible for the improved photocatalytic properties of the H:(STO/TiO$_2$). These results are consistent with those of previous XPS and Raman spectra.

On the basis of the above results, a possible mechanism to improve charge separation and transport over Au-sensitized H:(STO/TiO$_2$) heterostructures is proposed in Figure 7. Significantly, the band edges of the STO and TiO$_2$ are put into contact to form a type-II alignment and the conduction band and valence band of STO are at higher energy than those of TiO$_2$ so that under solar light irradiation the photoelectrons in the conduction band of STO migrate to the conduction band of TiO$_2$; at the same time, the photoholes in the valence band of TiO$_2$ move to the valence band of STO. The spatial separation of photoelectrons and photoholes in different units becomes thermodynamically favored, thus greatly preventing the recombination behavior. Once depositing Au on the surface of the H:(STO/TiO$_2$), under solar irradiation, the
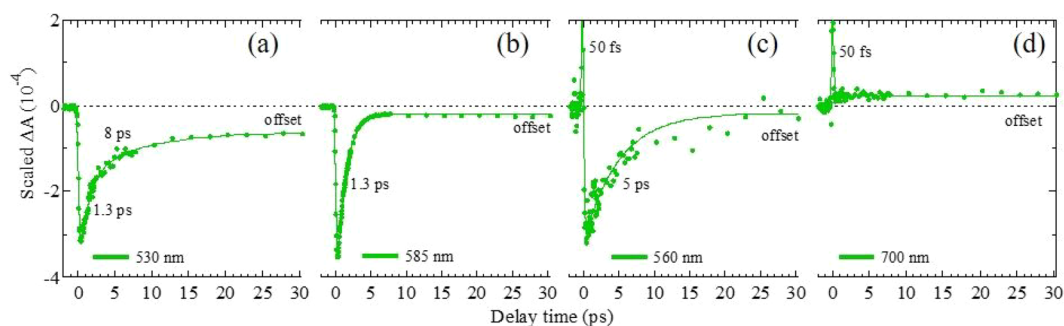
Figure 9. Femtosecond transient kinetic bands of Au NP monitored at (a) 530 nm for solution, (b) 585 nm for film, (c) 560, and (d) 700 nm for Au/H:(STO/TiO$_2$). The transient kinetic bands were fitted with two exponential functions.

electrons of STO and Au are photoexcited and then transferred to the conduction band of TiO$_2$. Meanwhile, the photoexcited holes in the valence band of TiO$_2$ are transferred to the valence band of STO and the Au surface. The synergistic effect between TiO$_2$ and STO with the modified electronic band structure significantly enhances an efficient charge transition and can diminish the recombination of charge carriers and prolong the charge lifetime under simulated sunlight irradiation. Furthermore, the vectorial electrons transfer rapidly through the aligned TiO$_2$ nanotube arrays, which facilitates charge transport and thus enhances the quantum efficiency and rate of H$_2$ evolution.

3.6. Ultrafast Electron Transfer Dynamics. The dynamic study of Au NP solution, Au NP thin-film, and Au/H:(STO/TiO$_2$) photoelectrodes is demonstrated in Figures 8 and 9. The Au NP solution and Au/H:(STO/TiO$_2$) was prepared as discussed in Section 2.1. The Au thin film was obtained via Au NP solution on a glass plate by repetitive drop method. The femtosecond TAS were measured using 480 nm excitation pulse and probed with a white-light pulse in the region between 520 and 730 nm. Figure 8a−c shows the evolution of the photobleach (PB) of the Au bands between 0−0.2 ps, while Figure 8d−f shows their subsequent recombination in the delay range 0.4−30 ps. The peak position of the Au plasmonic PB bands at 530 nm is consistent with that of the steady-state absorption spectrum (Figure S5), while the PB shows a redshift when Au NP were drop-casted or loaded into nanotubes. The PB band position in the film is at 585 nm, while its position in the nanotubes is 560 nm. The shift in the peak position of PB reflects the change in the refractive index of surrounding environments, while the band broadness is an indicator of the size distribution of Au NP. The Au NPs, when dispersed in a solvent, display a symmetric and narrow distribution, whereas when they were drop casted on glass substrates agglomeration results in a very broad PB band. Usually, the PB bands of Au plasmonic bands show photoinduced absorption (PIA) on both sides of the spectra and blue shift of the spectra with increased pump−probe delay time.[60,61] The spectra shown in Figure 8 do not cover the whole region of PIA bands, but their signatures can be observed clearly for the solution sample. The origin of the PIA bands and the blue shift of the PB band[62] can be explained based on the shift and broadening of the plasmon band due to the heating of the electron gas in Au NP during the decay of the plasmon band.[62,63,65]

Because of the plasmonic effect of excited Au NPs, a broad PIA band was noticed for the Au/H:(STO/TiO$_2$) film. By extending delay time to 30 ps, the transient kinetics[64] for the

PB bands of the corresponding three samples are shown in Figure 9. The data are fitted with two exponential functions. The transient kinetics reflect the hot carrier cooling process and subsequent recombination in Au NPs. In the case of solution and thin-film samples, cooling of hot carriers with a time coefficient 1.3 ps was observed while such a rapid cooling process was absent in the case of the Au/H:(STO/TiO$_2$) due to rapid injection of hot electrons from Au NP into the H:(STO/TiO$_2$). In the studies published elsewhere, the electron injection time was found to be less than 200 fs for TiO$_2$.[61,66] The rapid decay (1.3 ps component) of hot electrons in Au NPs is expressed based on electron−phonon interactions while the slower decay (5−8 ps component) can be associated with remaining electrons recombining via phonon−phonon interactions.[62] The hot-electron injection was probed by monitoring the transient kinetics at 700 nm, away from PB band of the Au NP as shown in Figure 9d. The rapid evolution of PIA bands can be understood as induced absorption in H:(STO/TiO$_2$) by the plasmonic effect via electron transfer, as plasmonic waves decay within 10 fs,[63] whereas the faster decay of PIA band within 50 fs can be understood as rapid trapping of injected electrons in conduction band to the surface states of H:(STO/TiO$_2$), which is close to the trapping decay coefficient of 100 fs reported for TiO$_2$ nanocrystalline films.[67] As the 700 nm region is known to have absorption for both free and trapped carriers in semiconductors,[67] we assign the PIA band to the free carriers in the conduction band of H:(STO/TiO$_2$) via hot electron injection from AuNP; however, its rapid decay is assigned to trapping by the surface states of H:(STO/TiO$_2$) because if PIA band is observed due to direct electron transfer from Au NP to the surface states of H:(STO/TiO$_2$), the decay would be slower. Thus, our fs TAS results provide direct evidence for plasmon-induced absorption of Au NPs and rapid injection of hot electrons into H:(STO/TiO$_2$) nanotubes. It is significant to note that the LSPR effect is dominant on the photocatalytic activity.

4. CONCLUSION

The heterocoupling of perovskite-type STO on TiO$_2$ nanotube arrays and plasmonic Au-decorating on Au/H:(STO/TiO$_2$) not only boosted their photoresponse under visible light but also facilitated efficient charge separation and transfer for photocatalytic production of hydrogen. Moreover, their synergistic effects substantially improved the photocatalytic performance for hydrogen production under simulated sunlight irradiation, which is nine times the photocatalytic capabilities of the pristine TiO$_2$ under the same conditions. With the aid of XAS in situ and TAS, the origin of this

enhancement was well elucidated. These findings might offer new insight into the design of highly efficient oxide-based photoelectrodes for photocatalytic hydrogen production.

■ ASSOCIATED CONTENT

Ⓢ Supporting Information

The Supporting Information is available free of charge at https://pubs.acs.org/doi/10.1021/acs.jpcc.1c05781.

> The XPS analyses; the XRD characterization; the SEM, TEM/HRTEM images of Au/H:(STO/TiO$_2$) NT arrays; IPCE spectra; UV−vis absorption spectra of aqueous Au NPs; gas evolution measurement; apparent quantum efficiency (PDF)

■ AUTHOR INFORMATION

Corresponding Authors

M. C. Lin − *Department of Applied Chemistry and Center for Emergent Functional Matter Science, National Yang Ming Chiao Tung University, Hsinchu 300093, Taiwan;* ⓞ orcid.org/0000-0003-3963-6017; Email: chemmcl@emory.edu

Yan-Gu Lin − *Scientific Research Division, National Synchrotron Radiation Research Center, Hsinchu 30076, Taiwan; Center for Emergent Functional Matter Science, National Yang Ming Chiao Tung University, Hsinchu 300093, Taiwan;* ⓞ orcid.org/0000-0002-4210-7709; Email: lin.yg@nsrrc.org.tw

Authors

Tsai-Te Wang − *Scientific Research Division, National Synchrotron Radiation Research Center, Hsinchu 30076, Taiwan;* ⓞ orcid.org/0000-0003-3976-6778

Chao-Lung Chiang − *Scientific Research Division, National Synchrotron Radiation Research Center, Hsinchu 30076, Taiwan*

Sudhakar Narra − *Department of Applied Chemistry and Center for Emergent Functional Matter Science, National Yang Ming Chiao Tung University, Hsinchu 300093, Taiwan;* ⓞ orcid.org/0000-0003-4893-9204

Jhih-Long Lin − *Department of Applied Chemistry, National Yang Ming Chiao Tung University, Hsinchu 300093, Taiwan*

Shao-Wen Chien − *Department of Applied Chemistry, National Yang Ming Chiao Tung University, Hsinchu 300093, Taiwan*

Jhin-Cheng Yu − *Department of Applied Chemistry, National Yang Ming Chiao Tung University, Hsinchu 300093, Taiwan*

Eric Wei-Guang Diau − *Department of Applied Chemistry and Center for Emergent Functional Matter Science, National Yang Ming Chiao Tung University, Hsinchu 300093, Taiwan;* ⓞ orcid.org/0000-0001-6113-5679

Complete contact information is available at:
https://pubs.acs.org/10.1021/acs.jpcc.1c05781

Author Contributions

‖T.-T.W. and C.-L.C. contributed equally.

Notes

The authors declare no competing financial interest.

■ ACKNOWLEDGMENTS

■ REFERENCES

(1) Grimes, C. A.; Varghese, O. K.; Ranjan, S. *Light, Water, Hydrogen: The Solar Generation of Hydrogen by Water Photoelectrolysis*; Springer: Norwell, MA; 2007.

(2) Fujishima, A.; Honda, K. Electrochemical Photolysis of Water at a Semiconductor Electrode. *Nature* **1972**, *238*, 37−38.

(3) Pesci, F. M.; Wang, G.; Klug, D. R.; Li, Y.; Cowan, A. J. Efficient Suppression of Electron-Hole Recombination in Oxygen-Deficient Hydrogen-Treated TiO$_2$ Nanowires for Photoelectrochemical Water Splitting. *J. Phys. Chem. C* **2013**, *117*, 25837−25844.

(4) Chen, S.; Xiao, Y.; Wang, Y.; Hu, Z.; Zhao, H.; Xie, W. A Facile Approach to Prepare Black TiO$_2$ with Oxygen Vacancy for Enhancing Photocatalytic Activity. *Nanomaterials* **2018**, *8*, 245−260.

(5) Chen, X.; Liu, L.; Yu, P. Y.; Mao, S. S. Increasing Solar Absorption for Photocatalysis with Black Hydrogenated Titanium Dioxide Nanocrystals. *Science* **2011**, *331*, 746−750.

(6) Chen, X.; Mao, S. S. Titanium Dioxide Nanomaterials: Synthesis, Properties, Modifications, and Applications. *Chem. Rev.* **2007**, *107*, 2891−2959.

(7) Zhu, K.; Neale, N. R.; Miedaner, A.; Frank, A. J. Enhanced Charge-Collection Efficiencies and Light Scattering in Dye-Sensitized Solar Cells Using Oriented TiO$_2$ Nanotubes Arrays. *Nano Lett.* **2007**, *7*, 69−74.

(8) Mor, G. K.; Shankar, K.; Paulose, M.; Varghese, O. K.; Grimes, C. A. Use of Highly-Ordered TiO$_2$ Nanotube Arrays in Dye-Sensitized Solar Cells. *Nano Lett.* **2006**, *6*, 215−218.

(9) Chen, X.; Burda, C. The Electroic Origin of the Visible-Light Absorption Properties of C-, N- and S- Doped TiO$_2$ Nanomaterials. *J. Am. Chem. Soc.* **2008**, *130*, 5018−5019.

(10) Wang, T. T.; Raghunath, P.; Lin, Y. C.; Lin, Y. G.; Lin, M. C. Effective Hydrogenation of TiO$_2$ Photocatalysts with CH$_3$OH for Enhanced Water Splitting: A Computational and X-ray Study. *Appl. Surf. Sci.* **2019**, *488*, 546−554.

(11) Wang, T. T.; Lin, Y. C.; Lin, M. C.; Lin, Y. G. Au-Assisted Methanol-Hydrogenated Titanium Dioxide for Photocatalytic evolution of Hydrogen. *Catal. Today* **2020**, *358*, 143−148.

(12) Wang, T. T.; Raghunath, P.; Lin, Y. G.; Lin, M. C. Synergistic Effect of Hydrogenation and Thiocyanate Treatments on Ag-Loaded TiO$_2$ Nanoparticles for Solar-to-Hydrogen Conversion. *J. Phys. Chem. C* **2017**, *121*, 9681−9690.

(13) Wang, T. T.; Chiang, C. L.; Lin, Y. C.; Srinivasadesikan, V.; Lin, M. C.; Lin, Y. G. KSCN-Activation of Hydrogenated NiO/TiO$_2$ for Enhanced Photocatalytic Hydrogen Evolution. *Appl. Surf. Sci.* **2020**, *511*, 145548−145554.

(14) Luo, Z.; Kriz, D. A.; Miao, R.; Kuo, C. H.; Zhong, W.; Guild, C.; He, J.; Willis, B.; Dang, Y.; Suib, S. L.; et al. TiO$_2$ Supported Gold-Palladium Catalyst for Effective Syngas Production from Methane Partial Oxidation. *Appl. Catal., A* **2018**, *554*, 54−63.

(15) Han, S.; Yu, L.; Zhang, H.; Chu, Z.; Chen, X.; Xi, H.; Long, J. Gold Plasmon-Enhanced Solar Hydrogen Production over STO/TiO$_2$ Heterostructures. *ChemCatChem* **2019**, *11*, 6203−6207.

(16) Wang, M.; Li, S.; Lv, Y.; Zhou, X. Theoretical Insights into Interfacial and Electronic Structures of NiO$_x$/STO Photocatalyst for Overall Water Splitting. *J. Energy Chem.* **2019**, *33*, 138−148.

(17) Ouyang, S.; Tong, H.; Umezawa, N.; Cao, J.; Li, P.; Bi, Y.; Zhang, Y.; Ye, J. Surface-Alkalinization-Induced Enhancement of Photocatalytic H$_2$ Evolution over STO-Based Photocatalysts. *J. Am. Chem. Soc.* **2012**, *134*, 1974−1977.

(18) Mehnane, H. F.; Wang, C.; Kondamareddy, K. K.; Yu, W.; Sun, W.; Liu, H.; Bai, S.; Liu, W.; Guo, S.; Zhao, X. Z. Hydrothermal Synthesis of TiO_2 Nanoparticles Doped with Trace Amounts of Strontium, and Their Application as Working Electrodes for Dye Sensitized Solar Cells: Tunable Electrical Properties & Enhanced Photo-Conversion Performance. *RSC Adv.* **2017**, 7, 2358−2364.

(19) Zhang, J.; Bang, J. H.; Tang, C.; Kamat, P. V. Tailored TiO_2-STO Heterostructure Nanotube Arrays for Improved Photoelectrochemical Performance. *ACS Nano* **2010**, 4, 387−395.

(20) Zhang, J.; Tang, C.; Bang, J. H. CdS/TiO_2-STO Heterostructure Nanotube Arrays for Improved Solar Energy Conversion Efficiency. *Electrochem. Commun.* **2010**, 12, 1124−1128.

(21) Hamedani, H. A.; Allam, N. K.; Garmestani, H.; El-Sayed, M. A. Electrochemical Fabrication of Strontium-Doped TiO_2 Nanotube Array Electrodes and Investigation of Their Photoelectrochemical Properties. *J. Phys. Chem. C* **2011**, 115, 13480−13486.

(22) Linic, S.; Christopher, P.; Ingram, D. B. Plasmonic-Metal nanostructures for Efficient Conversion of Solar to Chemical Energy. *Nat. Mater.* **2011**, 10, 911−921.

(23) Xiao, M.; Jiang, R.; Wang, F.; Fang, C.; Wang, J.; Yu, J. C. Plasmon-Enhanced Chemical Reactions. *J. Mater. Chem. A* **2013**, 1, 5790−5805.

(24) Baffou, G.; Quidant, R. Nanoplasmonics for Chemistry. *Chem. Soc. Rev.* **2014**, 43, 3898−3907.

(25) Jiang, R.; Li, B.; Fang, C.; Wang, J. Metal/Semiconductor Hybrids Nanostructures for Plasmon-Enhanced Applications. *Adv. Mater.* **2014**, 26, 5274−5309.

(26) Shi, Xu; Ueno, K.; Oshikiri, T.; Sun, Q.; Sasaki, K.; Misawa, H. Enhanced Water Splitting Under Modal Strong Coupling Conditions. *Nat. Nanotechnol.* **2018**, 13, 953−958.

(27) Serra, M.; Albero, J.; Garcia, H. Photocatalytic Activity of Au/TiO_2 Photocatalysts for H_2 Evolution: Role of the Au Nanoparticles as a Function of the Irradiation Wavelength. *ChemPhysChem* **2015**, 16, 1842−1845.

(28) Tian, Y.; Tatsuma, T. Mechanisms and Applications of Plasmon-Induced Charge Separation at TiO_2 Films Loaded with Gold Nanoparticles. *J. Am. Chem. Soc.* **2005**, 127, 7632−7637.

(29) Huang, J. R.; Tan, X.; Yu, T.; Hu, W. L.; Zhao, L.; Liu, H.; Zhang, L.; Zou, Y. L. N-Doped TiO_2/STO Heterostructured Nanotubes for High-Efficiency Photoelectrocatalytic Properties under Visible-Light Irradiation. *ChemElectroChem* **2015**, 2, 1174−1181.

(30) Liu, L.; Li, P.; Wang, T.; Hu, H.; Jiang, H.; Liu, H.; Ye, J. Constructing a Multicomponent Junction for Improved Visible-Light Photocatalytic Performance induced by Au Nanoparticles. *Chem. Commun.* **2015**, 51, 2173−2176.

(31) Wang, B.; Li, R.; Zhang, Z.; Zhang, W.; Yan, X.; Wu, X.; Cheng, G.; Zheng, R. Novel Au/Cu_2O Multi-Shell Porous Heterosturctures for Enhanced Efficiency of Photoelectrochemical Water Splitting. *J. Mater. Chem. A* **2017**, 5, 14415−14421.

(32) Zhang, W. F.; He, Y. L.; Zhang, M. S.; Yin, Z.; Chen, Q. Raman Scattering Study on Anatase TiO_2 Nanocrystals. *J. Phys. D: Appl. Phys.* **2000**, 33, 912−916.

(33) Frank, O.; Zukalova, M.; Laskova, B.; Kurti, J.; Koltai, J.; Kavan, L. Raman Spectra of Titatium Dioxide (Anatase, Rutile) with Identified Oxygen Isotopes (16,17,18). *Phys. Chem. Chem. Phys.* **2012**, 14, 14567−14572.

(34) Rahman, M. Y. A.; Samsuri, S. A. M.; Umar, A. A. TiO_2-STO Composite Photoanode: Effect of Strontium Precursor Concentration on the Performance of Dye-Sensitized Solar Cells. *Appl. Phys. A: Mater. Sci. Process.* **2019**, 125, 59−69.

(35) Mishra, P. R.; Shukla, P. K.; Srivastava, O. N. Study of Modular PEC Solar Cells for Photoelectrochemical Splitting of Water Employing Nanostructrued TiO_2 Photoelectrodes. *Int. J. Hydrogen Energy* **2007**, 32, 1680−1685.

(36) Pougin, A.; Luken, A.; Klinkhammer, C.; Hiltrop, D.; Kauer, M.; Tolle, K.; Havenith-Newen, M.; Morgenstern, K.; Grunert, W.; Muhler, M.; Strunk, J.; et al. Probing Oxide Reduction and Phase Transformation at the Au-TiO_2 Interface by Vibrational Spectroscopy. *Top. Catal.* **2017**, 60, 1744−1753.

(37) Nilsen, W. G.; Skinner, J. G. Raman Spectrum of Strontium Titanate. *J. Chem. Phys.* **1968**, 48, 2240−2248.

(38) Merkulov, V. I.; Fox, J. R.; Li, H. C.; Si, W.; Sirenko, A. A. Metal-oxide Bilayer Raman Scattering in STO Thin Film. *Appl. Phys. Lett.* **1998**, 72, 3291−3293.

(39) Pang, Y.; Xu, G.; Feng, Q.; Lv, J.; Qin, Y.; Zhang, Y.; Zheng, Z.; Wu, Y. Crystalline Orientation Preference for TiO_2 Nanotube Arrays with Efficient Photoelectrochemical Properties. *Phys. Lett. A* **2018**, 382, 2759−2762.

(40) Xian, T.; Di, L.; Sun, X.; Ma, J.; Zhou, Y.; Wei, X. Photocatalytic Degration of Dyes over Au Decorated STO Nanoparticles under Simulated Sunlight and Visible Light Irradiation. *J. Ceram. Soc. Jpn.* **2018**, 126, 354−359.

(41) Bar-Ziv, R.; Ranjan, P.; Lavie, A.; Jain, A.; Garai, S.; Bar Hen, A.; Popovitz-Biro, R.; Tenne, R.; Arenal, R.; Ramasubramaniam, A.; Lajaunie, L.; Bar-Sadan, M.; et al. Au-MoS_2 Hybrids as Hydrogen Evolution Electrocatalysts. *ACS Appl. Energy Mater.* **2019**, 2, 6043−6050.

(42) Xing, G.; Zhao, L.; Sun, T.; Su, Y.; Wang, X. Hydrothermal Driven Nitrogen Doped STO for Efficient Visible Light Driven Photocatalytic Reduction of Chromium (VI). *SpringerPlus* **2016**, 5, 1132−1144.

(43) Ku, Y.; Lin, C. N.; Hou, W. M. Characterization of Coupled NiO/TiO_2 Photocatalyst for the Photocatalytic Reduction of Cr (VI) in Aqueous Solution. *J. Mol. Catal. A: Chem.* **2011**, 349, 20−27.

(44) Su, F.; Wang, T.; Lv, R.; Zhang, J.; Zhang, P.; Lu, J.; Gong, J. Dendritic Au/TiO_2 Nanorod Arrays for Visible-light-driven Photoelectrochemical Water Splitting. *Nanoscale* **2013**, 5, 9001−9009.

(45) Wang, J.; Wang, Z.; Huang, B.; Ma, Y.; Liu, Y.; Qin, X.; Zhang, X.; Dai, Y. Oxygen Vacancy Induced Band-gap Narrowing and Enhanced Visible Light Photocatalytic Activity of ZnO. *ACS Appl. Mater. Interfaces* **2012**, 4, 4024−4030.

(46) Sood, S.; Umar, A.; Mehta, S. K.; Sinha, A. S. K.; Kansal, S. K. Efficient Photocatalytic Degradation of Brilliant Green Using Sr-doped TiO2 Nanoparticles. *Ceram. Int.* **2015**, 41, 3533−3540.

(47) Antuch, M.; Millet, P.; Iwase, A.; Kudo, A. Water Reduction into Hydrogen Using Rh-doped STO Photoelectrodes Surface-Modified by Minute Amounts of Pt: Insights from Heterogeneous Kinetic Analysis. *Electrochim. Acta* **2019**, 297, 696−704.

(48) Ke, X.; Zhang, X.; Zhao, J.; Sarina, S.; Barry, J.; Zhu, H. Selective Reductions using Visible Light Photocatalysts of Supported Gold Nanoparticles. *Green Chem.* **2013**, 15, 236−244.

(49) Sugavaneshwar, R. P.; Chen, K.; Lakshminarayana, G.; Ishii, S.; Dao, T. D.; Umezawa, N.; Nagao, T. Plasmon Mediated Cathodic Photocurrent Generation in sol-gel Synthesized Doped STO Nanofilms. *APL Mater.* **2015**, 3, 116103−116108.

(50) Clavero, C. Plasmon-Induced Hot-Electron Generation at Nanoparticle/metal-oxide Interfaces for Photovoltaic and Photocatalytic Devices. *Nat. Photonics* **2014**, 8, 95−103.

(51) McCrory, C. C. L.; Jung, S.; Ferrer, I. M.; Chatman, S. M.; Peters, J. C.; Jaramillo, T. F. Benchmarking Hydrogen Evolving Reaction and Oxygen Evolving Reaction Electrocatalysts for Solar Water Splitting Devices. *J. Am. Chem. Soc.* **2015**, 137, 4347−4357.

(52) Kuo, H. W.; Lin, C. J.; Do, H. Y.; Wu, R. Y.; Tseng, C. M.; Kumar, K.; Dong, C. L.; Chen, C. L. Electronic and Atomic Structure of TiO_2 Anatase Spines on Sea-Urchin-Like Microspheres by X-ray Absorption Spectroscopy. *Appl. Surf. Sci.* **2020**, 502, 144297−144302.

(53) Paul, A.; Zheng, J. G.; Aoki, T. Titanium Magnetic Polarization at the Fe/BaTiO_3 Interfaces: An Effect of Ferroelectirc Polarization Discontinuity. *J. Appl. Phys.* **2017**, 122, 154302−157312.

(54) Jahn, H. A.; Teller, E. Stability of Polyatomic Molecules in Degenerate Electoinc States. *Proc. R. Soc. London A* **1937**, 161, 220−235.

(55) Nayak, C.; Bhattacharyya, D.; Bhattacharyya, K.; Tripathi, A. K.; Bapat, R. D.; Jha, S. N.; Sahoo, N. K. Insight into growth of Au−Pt bimetallic nanoparticles: an in situ XAS study. *J. Synchrotron Radiat.* **2017**, 24, 825−835.

(56) Li Bassi, A.; Cattaneo, D.; Russo, V.; Bottani, C. E.; Barborini, E.; Mazza, T.; Piseri, P.; Milani, P.; Ernst, F. O.; Wegner, K.; Pratsinis, S. E.; et al. Raman Spectroscopy Characterization of Titania Nanoparticles Produced by Flame Pyrolysis: The Influence of Size and Stoichiometry. *J. Appl. Phys.* **2005**, *98*, 074305−074313.

(57) Ekoi, E. J.; Gowen, A.; Dorrepaal, R.; Dowling, D. P. Characterisation of Titanium Oxide Layers Using Raman Spectroscopy and Optical Profilometry: Influence of Oxide Properties. *Results Phys.* **2019**, *12*, 1574−1585.

(58) Wang, T. T.; Yang, Y. T.; Lim, S. C.; Chiang, C. L.; Lim, J. S.; Lin, Y. C.; Peng, C. K.; Lin, M. C.; Lin, Y. G. Hydrogenation Engineering of Bimetallic Ag-Cu-Modified-Titania Photocatalysts for Production of Hydrogen. *Catal. Today* **2021**, DOI: 10.1016/j.cattod.2020.11.012.

(59) Jiang, P.; Prendergast, D.; Borondics, F.; Porsgaard, S.; Giovanetti, L.; Pach, E.; Newberg, J.; Bluhm, H.; Besenbacher, F.; Salmeron, M. Experimental and Theoretical Investigation of the Electronic Structure of Cu_2O and CuO Thin Films on Cu (110) Using X-ray Photoelectron and Absorption Spectroscopy. *J. Chem. Phys.* **2013**, *138*, 024704−024709.

(60) Xing, Z.; Liu, Q.; Asiri, A. M.; Sun, X. High-Efficiency Elcectrochemical Hydrogen Evolution Catalyzed by Tungsten Phosphide Submicroparticles. *ACS Catal.* **2015**, *5*, 145−149.

(61) Hattori, Y.; Abdellah, M.; Meng, J.; Zheng, K.; Sá, J. Simultaneous Hot Electron and Hole Injection upon Excitation of Gold Surface Plasmon. *J. Phys. Chem. Lett.* **2019**, *10*, 3140−3146.

(62) Link, S.; El-Sayed, M. A. Optical Properties and Ultrafast Dynamics of Metallic Nanocrystals. *Annu. Rev. Phys. Chem.* **2003**, *54*, 331−366.

(63) Saavedra, J. R. M.; Asenjo-Garcia, A.; Garcia de Abajo, F. J. Hot-Electron Dynamics and Thermalization in Small Metallic Nanoparticles. *ACS Photonics* **2016**, *3*, 1637−1646.

(64) Narra, S.; Jokar, E.; Pearce, O.; Lin, C.-Y.; Fathi, A.; Diau, E. W.-G. Femtosecond Transient Absorption Spectra and Dynamics of Carrier Relaxation of Tin Perovskites in the Absence and Presence of Additives. *J. Phys. Chem. Lett.* **2020**, *11*, 5699−5704.

(65) Zhang, X.; Huang, C.; Wang, M.; Huang, P.; He, X.; Wei, Z. Transient Localized Surface Plasmon Induced by Femtosecond Interband Excitation in Gold Nanoparticles. *Sci. Rep.* **2018**, *8*, 10499−10505.

(66) Furube, A.; Du, L.; Hara, K.; Katoh, R.; Tachiya, M. Ultrafast Plasmon-Induced Electron Transfer from Gold Nanodots into TiO_2 Nanoparticles. *J. Am. Chem. Soc.* **2007**, *129*, 14852−14853.

(67) Tamaki, Y.; Hara, K.; Katoh, R.; Tachiya, M.; Furube, A. Femtosecond Visible-to-IR Spectroscopy of TiO_2 Nanocrystalline Films: Elucidation of the Electron Mobility before Deep Trapping. *J. Phys. Chem. C* **2009**, *113*, 11741−11746.